Effect of Interaction with H_2O and NH_3 on the Vibrational, Electronic, and Energetic Peculiarities of Ti(IV) Centers TS-1 Catalysts: A Spectroscopic and Computational Study

Silvia Bordiga,* Alessandro Damin, Francesca Bonino, and Adriano Zecchina

Dipartimento di Chimica, IFM Università di Torino, Via P. Giuria 7, 10125 Torino, Italy

Guido Spanò and Franco Rivetti

Polimeri Europa s.r.l. Centro Ricerche Novara, Istituto G. Donegani, Via G. Fauser 4, I-28100 Novara, Italy

Vera Bolis

Dipartimento di Scienze Chimiche, Alimentari, Farmaceutiche e Farmacologiche, Università del Piemonte Orientale "A. Avogadro", Via Bovio 6, 28100 Novara, Italy

Carmelo Prestipino and Carlo Lamberti

Dipartimento di Chimica, IFM Università di Torino, and INFM UdR Torino Università, Via P. Giuria 7, 10125 Torino, Italy

Received: May 13, 2002; In Final Form: June 25, 2002

In this work we present an exhaustive, experimental and theoretical, investigation on the structural, vibrational, electronic, and energetic properties of TS-1 catalyst. The perturbation induced by adsorption of water and ammonia ligands, which represent two key molecules in the industrial processes catalyzed by TS-1, is also discussed in great detail on both experimental and computational ground. Theory and experiments allow us to present a picture able to describe in a satisfactory way the interaction of both molecules with Ti(IV) sites and with the hosting siliceous matrix.

1. Introduction

Titanium silicalite-1 (TS-1) is a synthetic zeolite[1] in which a small number of Ti atoms substitute tetrahedral Si atoms in a purely siliceous framework with the MFI structure.[2] It is an active and selective catalyst in a number of low-temperature oxidation reactions with aqueous H_2O_2 as the oxidant.[3−9] For this reason, it has been one of the most studied materials in heterogeneous catalysis in the last years.

Several experimental[10−40] and computational[15,16,25,41−53] results demonstrate that the substitution of Si by Ti is isomorphous in well-prepared samples, and it is generally believed that the distribution of Ti over the available framework sites is at least partially disordered. Among these we quote vibrational spectroscopies (both IR and Raman),[16−27] UV−vis,[21,25,27,32,33] EXAFS,[27−37] and XANES,[27−29,31,33,34,36−38] spectroscopies, microcalorimetric measurements,[36,37] and powder diffraction experiments (using both X-rays and neutrons).[10−15]

Most of the quoted papers refer to dehydrated TS-1: such studies have reported important proofs describing the nature of the Ti active center. It is, however, evident that the next generation of experiments must be designed to investigate the catalyst in reactive conditions. In this work we move along this direction by reporting a detailed computational and experimental study on the interaction of TS-1 with H_2O and NH_3. Interaction with water is important because the catalyst works in aqueous solution. The interest in the study of NH_3 is 2-fold: ammonia is a reactant in the ammoximation of cyclohexanone to give cyclohexanone oxime and it is a stronger base than water, thus allowing a direct comparison between the effects induced by Lewis bases of increasing strength.

Interaction of probe molecules has been faced in some papers reporting either experimental[16,17,19,25,27,31,36−38] or theoretical[16,48,50−53] results. But a complete work reporting the effect of NH_3 and H_2O adsorption on the vibrational, electronic, and energetic features of Ti(IV) centers in TS-1 on both experimental and theoretical ground is still missing. This is the aim of the present study which is structured as follows. Sections 2.1, 2.2, and 2.3 are devoted to the description of the catalyst synthesis, the experimental details and the computational methods, respectively. Section 3.1 reports on the vibrational data (IR and Raman); sections 3.2, 3.3, and 3.4 concern UV−vis, microcalorimetric, and X-ray absorption (both XANES and EXAFS) experiments.

Finally, section 4 reports the computational results on the interaction between H_2O and NH_3 Lewis bases with the different models mimicking Ti(IV) Lewis centers in zeolites. Besides the comparison among the different Ti(IV) models, the computational results have been used either to confirm or to revise previous assignments of the experimental features. The agreement between computed and experimentally observed features is underlined, as well as the two main limits of the proposed computational study. (i) The former concerns the fact that the used clusters refer only to "perfect" Ti(IV) centers, i.e., Ti atoms linked to four Si through four oxygen bridges. This assumption means that we neglect the presence of "defective" sites where one or more Ti−O−Si bridges are hydrolyzed to give TiOH and HOSi pairs. The presence of hydroxylated cavities has been proved for the Ti-free structure[19,25,54−56] and for TS-1.[13,19,25,27,32,35−47] On this basis, it has been hypothesized

* To whom correspondence should be addressed:.Tel: +39011-6707858. Fax: +39011-6707855. E-Mail: silvia.bordiga@unito.it.

10.1021/jp026106t CCC: $22.00
Published on Web 08/29/2002

(but never directly demonstrated) that TiOH groups could be involved too. (ii) The latter is related to the inability of the model to treat the interaction with more than one adsorbed molecule.[57] As a consequence, the cooperative effects, which can be relevant for a system working in aqueous conditions, cannot be considered. Despite all these facts, the global approach presented here will lead to a satisfactory understanding of the complete set of experimental data collected in this work.

2. Experimental Section

2.1. Synthesis. A TS-1 sample has been synthesized in EniChem (now *Polimeri Europa*) laboratories following a procedure described in the original patent.[1] The Ti-content, *x*, expressed in TiO_2 wt %, has been found to be 3.0. For comparison, also a Ti-free silicalite has been synthesized in the same conditions. The complete insertion of Ti atoms in the MFI framework has been proved by comparison of the amount of Ti determined by chemical analysis with the cell volumes obtained by Rietveld refinement of powder XRD data; see ref 11 for more details. The absence of extraframework TiO_2 particles has been proved by UV−vis and XANES spectroscopies (vide infra) and by the absence of the 144 cm^{-1} Raman band (spectra not reported for brevity). In fact, the 144 cm^{-1} band, very strong in the Raman spectra of TiO_2, has been used for more than 10 years to detect even small traces of extraframework Ti in titanosilicates[21,58,59] and thus to distinguish between high- and low-quality TS-1 samples.

2.2. Characterization Techniques. For IR spectra a Brucker IFS 66 FTIR spectrometer equipped with an HgCdTe cryodetector has been used. For all spectra a resolution of 2 cm^{-1} has been adopted. Samples have been studied in transmission mode on thin self-supported wafers. Adsorbates have been dosed in the gas phase through a vacuum manifold directly connected with the measure cell on a TS-1 sample previously activated at 400 °C for 30 min in a dynamical vacuum of 10^{-4} Torr.

The conventional Raman spectra were obtained on a Perkin-Elmer 2000 NIR-FT Raman spectrometer equipped with an InGaAs detector. The lasing medium was an Nd:YAG crystal pumped by a high-pressure krypton lamp, resulting in an excitation wavelength of 1064 nm (9398 cm^{-1}). The power output was ca. 1000 mW. Raman spectra were collected on samples before and after being wetted with water or with ammoniacal solution. The diffuse reflectance UV−vis spectra were obtained on a Varian Cary 5 spectrometer.

The heats of adsorption of H_2O and NH_3 were measured at 303 K by means of a heat-flow microcalorimeter (standard Tian-Calvet type, Setaram-France) following a well-established stepwise procedure, previously described.[36,37,60] The equilibrium pressure was monitored by means of a transducer gauge (Barocel-Edwards 0−100 Torr, 1 Torr ≈ 133.3 Pa) enabling accurate measurements up to ca. 90 Torr (±0.01 Torr). The calorimeter was connected to a high-vacuum ($P \leq 10^{-5}$ Torr) gas-volumetric glass apparatus, that enabled us to determine simultaneously the adsorbed amounts (Δn_{ads}) and the heats evolved (ΔQ^{int}) for small increments of the adsorptive. Thanks to the differential construction of the apparatus, all parasite effects other than the one due to the interaction of the gas with the surface of the solid studied could be compensated. The adsorbed amounts ($n_{ads} = \Sigma \Delta n_{ads}$) and the integral heats evolved ($Q^{int} = \Sigma \Delta Q^{int}$) were so determined at increasing equilibrium pressure of the adsorptive. The amounts adsorbed and the integral heat evolved (per gram of sample) are reported as a function of the equilibrium pressure of the probe giving rise to the volumetric (n_{ads} vs P) and to the calorimetric (Q^{int} vs P) isotherms, respectively. The integral heats evolved during the adsorption process will be reported also as a function of the increasing adsorbed amounts (Q^{int} vs n_{ads}). The differential heat of adsorption (q^{diff}) is defined as the first derivative of the Q^{int} curves taken against n_{ads}. A polynomial of the form $Q^{int} = \Sigma a_k (n_{ads})^k$ was used to fit by least squares the integral heat curves, giving directly $q^{diff} = \Sigma k a_k (n_{ads})^{k-1}$. Alternatively, q^{diff} can be obtained by taking the middle points of the experimental histogram of the partial molar heats ($\Delta Q^{int}/\Delta n_{ads}$, kJ/mol) for incremental doses of the adsorptive as a function of the adsorbed amounts n_{ads}. Whatever method is employed, the differential heats of adsorption are reported as a function of the coverage (q^{diff} vs n_{ads}).

A first run of adsorption was performed on the samples previously outgassed at 673 K (2 h, 10^{-5} Torr) and then transferred into the calorimeter without further exposure to the atmosphere. A second run was performed after outgassing the sample at the calorimeter temperature overnight (≈15 h, at 10^{-5} Torr), to evaluate the contribution of the reversible (in the adopted conditions) component to the adsorption. In the present work only the second run data will be reported, as discussed in the text (vide infra).

XAFS spectra were performed in the transmission mode, at the EXAFS13 beam line of the DCI storage ring (operating at 1.85 GeV with a typical current of 300 mA) of LURE laboratories in Orsay (F), using air-filled ionization chambers for both incident and transmitted beams. For both detectors the gas pressure was optimized ad hoc for each sample, maximizing the measured current within the linearity region of the device. The incident beam was monochromatized using a double crystal Si(111) (Si(311)) with a sampling step of 2.0 eV (0.5 eV) and an integration time of 2.0 s/point (1.0 s/point) for EXAFS (XANES) spectra. For both experimental setups the energy/angle calibration was performed using a Ti foil and crystals were detuned up to half of the rocking curve to avoid harmonics. To follow the modification of the local environment around Ti centers upon interaction with H_2O and NH_3 adsorbates, EXAFS (XANES) spectroscopy was performed using an iron cell ad hoc designed by the authors to allow measurements under a carefully controlled atmosphere where the sample could be introduced in the form of thin self-supporting wafers. Pellet homogeneity was controlled by the uniformity of the X-ray beam transmitted through the sample by radiographic methods. This cell, equipped with two Mylar windows, could be connected to a vacuum line for sample pretreatment (high-temperature activation in dynamic vacuum) and to a high-purity line for gas dosage. For the TS-1 sample in each condition (in a vacuum or in the presence of different P_{H_2O} and P_{NH_3}) the EXAFS spectrum was acquired four times under the same experimental conditions: from the four extracted $\chi_i(k)$ ($i = 1-4$) the average $\chi(k) = (1/4)\Sigma_{i=1}^{4} \chi_i(k)$ function was computed and used for the data analysis. The analysis of the EXAFS data was done at two different levels.

Level one corresponds to a standard single scattering fit of the first shell environment around Ti. It was carried out using programs developed by Michalowicz[61] and following standard procedures.[62] The Ti−O phase and amplitude function have been extracted from the TiO_2 (anatase) model compound and have been used to simulate also Ti−N shells. This approximation is acceptable, because oxygen and nitrogen scatterers differ in only one electron.[36,37] A similar approximation was used for the Cu−O and Cu−C shells.[63] An extensive description of both experimental conditions and data analysis can be found in ref 32.

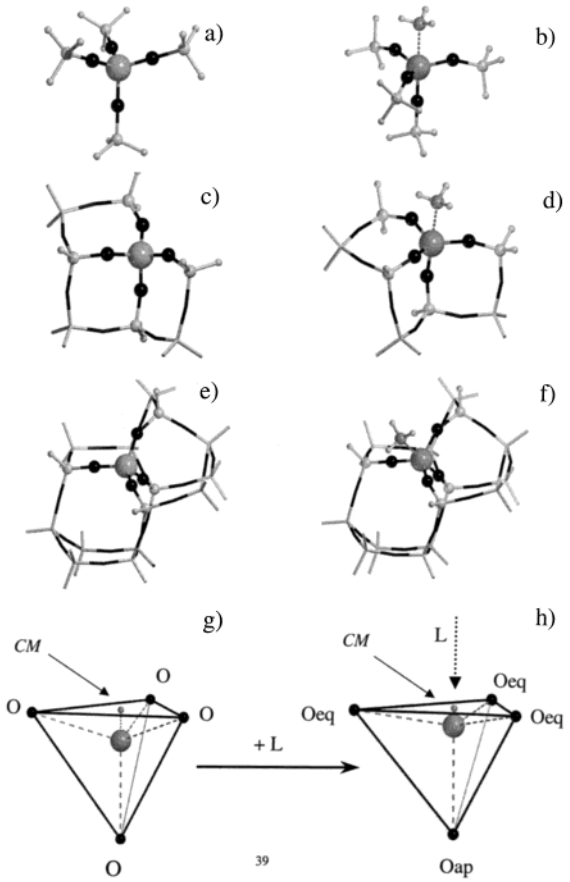

Figure 1. T5 ($TiO_4Si_4H_{12}$), CHA_T8 ($TiSi_7O_{10}H_{12}$), and MFI_T16 ($TiSi_{15}O_{22}H_{20}$) bare cluster models, parts a, c, and e, respectively. Parts b, d, and f as parts a, c, and e for the clusters engaged with NH_3. For clusters CHA_T8 and MFI_T16 sticks and balls vs sticks notation discriminates the model zone (where the link H atoms are omitted for clarity) from the complementary part of the cluster treated at low level only. Gray, black, and white colors define Ti, O, and (Si or H) atoms. Ammonia is represented in sticks and balls, and its interaction with the Ti(IV) centers is represented by dots. Part g reports a schematic representation of the Ti(IV) first shell (TiO_4 unit) center in T_d symmetry, whereas part h represents the deformation of the tetrahedron by ligand insertion. The dotted arrow represents the absorption direction of the ligand molecule (L = H_2O or NH_3), which breaks the symmetry of the four first neighbor oxygen atoms into three equatorial (O_{eq}) and one apical (O_{ap}). The small gray sphere shows the center of mass of the three O_{eq} atoms (labeled as the CM point in the text).

Level two is based on the simulation of the EXAFS signal generated by FEFF8 code[64] on the clusters optimized by ab initio methods (vide infra section 2.3). The results reported in this second level are only preliminary because we are only dealing with simulations and not with fits. Notwithstanding this fact, these simulations will be important to support our thesis. For the purposes presented in this work the constant amplitude factor S_0^2 and the Debye−Waller factors σ have been arbitrarily set to 1.0 and 0.0, respectively for all paths. In the FEFF8 simulation we have included all single and multiple paths within half the path length of 4.2 Å and with an intensity higher than 3% that of the stronger path. For the MFI_T16 ($TiSi_{15}O_{22}H_{20}$) cluster (vide infra section 2.3) in interaction with water and ammonia this approach yields to 41 and 42 paths, respectively.

2.3. Models and Computational Details. In this work three cluster models are used to simulate the "perfect" Ti site in TS-1 and to study its interaction toward H_2O and NH_3 molecules. We have here omitted the minimal $Ti(OH)_4$ one (treated in refs 50 and 65), considering the $Ti(OSiH_3)_4$ (hereafter named as model T5, see Figure 1a) as the simplest cluster. Model T5, already treated in refs 51, 53, 65, and 66, does not consider any environmental constraint due to the insertion in a zeolitic framework. To partially overcome this problem, some of the quoted authors[51,53] have fixed the position of the second (Si) and third (H) shell. It is, however, evident that a more realistic way to face this problem consists of employing bigger clusters obtained by cutting suitable portions from real zeolitic frameworks. Following this approach we have used in this work clusters CHA_T8 ($TiSi_7O_{10}H_{12}$) and MFI_T16 ($TiSi_{15}O_{22}H_{20}$), which have been obtained from the chabazite and the MFI (site T1, see ref 13) structures, respectively. Clusters T5, CHA_T8, and MFI_T16 are reported in Figure 1a,c,e, respectively. This nomenclature comes from ref 67, which makes a systematic methodological comparison among $Ti(OH)_4$ (model T1), T5, $TiSi_6O_8H_{12}$ (model T7), CHA_T8, $TiSi_{13}O_{19}H_{18}$ (model MFI_T14), $TiSi_{14}O_{20}H_{20}$ (model MFI_T15), MFI_T16, and $TiSi_{17}O_{26}H_{20}$ (model MFI_T18).

Moving from model T5 to models CHA_T8 and MFI_T16, the number of involved atoms increases significantly. To limit the computational demand, in our calculations, the cluster/embedded cluster ONIOM[68] scheme based on the integration of molecular orbital at different levels of theory is employed.[68b]

Basically, the ONIOM scheme allows us to treat at different levels of theory (and so at different computational costs) different parts of a large cluster. A higher level of theory can so be applied on a smaller portion of the whole cluster (containing up to the second shell around Ti in our case: ball-and-sticks in Figure 1) only, the remaining atoms (sticks in Figure 1) being treated at a lower level of theory. In the ONIOM literature the high-level zone is often referred as the model zone. The electroneutrality of the model zone is obtained by saturating dangling bonds with the so-called "link-atoms" (H atoms in our case), not shown in Figure 1 for the sake of simplicity. A portion (defined as the model part M: stick and balls in Figure 1) is extracted from the large cluster (the real system R). In the present case the total energy of the ONIOM system (E(ONIOM)) is obtained from three distinct self-consistent field energy calculations that are combined according to the following equation:

$$E(\text{ONIOM}) = E_{\text{High}}(\text{model zone}) + [E_{\text{Low}}(\text{whole cluster}) - E_{\text{Low}}(\text{model zone})] \quad (1)$$

where E_{Low}(whole cluster) is the energy of the whole cluster calculated at the low level of theory (RHF/3-21G(H,N,Si,O), 3-21G*(Ti)), E_{Low}(model zone) is the energy of the model zone computed at the low level of theory (RHF/3-21G(H,N,Si,O), 3-21G*(Ti)), and E_{High}(model zone) is the energy of the model zone computed at the high level of theory at the (B3-LYP/6-311+G(d,p)(H,N,Si,O), ppp(Ti)) high (H) level. Here, ppp represents the basis-set employed for the Ti atom: it is composed of effective small core pseudopotentials[69] + LANL2DZ[69] + Ahlrichs TZV "p" polarization function.[70] As the geometry optimization is based on the minimization of E(ONIOM) energy, it is obtained according to the recombination of three distinct gradient calculations.

To allow a direct comparison among the computational results obtained with the three models, the model zone (including link atoms) of both clusters CHA_T8 and MFI_T16 is the $Ti(OSiH_3)_4$ cluster of model T5. Of course, model T5 has been computed ab initio using the same basis set employed for the high-level model calculations. The starting coordinates for the structural optimization of both CHA_T8 and MFI_T16 clusters are those obtained from crystallographic data. During the optimization

cycles all atomic positions were free to relax without any artificial constraints imposed on the model zone excepted those induced by the whole cluster itself. This role is played by the link atoms who transfer mechanical constraints from the whole cluster to the model zone. In fact, link atoms are forced to stay along the Si−O directions (Si being the last atom of the model zone and O the first atom of the zone treated at lower level).

The absorption of a ligand molecule breaks the symmetry (T_d for cluster T5) around Ti(IV) center (Figure 1g). In this regard, the four oxygen atoms are no more equivalent and must be divided into three equatorial ones and an apical one (O_{eq} and O_{ap} in Figure 1h). The three O_{eq} define the plane perpendicular to the adsorption direction, whereas O_{ap} lies on the opposite side with respect to the adsorbed molecule. This implies that the six O−Ti−O angles of the TiO_4 unit are no more equivalent upon adsorption, even for the T5 cluster. For this reason we label with α the three $O_{eq}-Ti-O_{eq}$ angles and with β the three $O_{eq}-Ti-O_{ap}$ angles. The center of mass of the three O_{eq} atoms is labeled as CM. The Ti−CM distance moves from Ti−O cos(70.5°) in T_d symmetry (being 70.5° = 180− 109.5°) to zero in a perfect bipyramidal symmetry (where the Ti atom lies in the plane defined by the three O_{eq} atoms). As a consequence the Ti−CM distance gives a direct measure of the symmetry distortion undergone by the TiO_4 moiety upon insertion in a portion of the zeolite framework (models CHA_T8 and MFI_T16) and upon absorption of a ligand molecule.

Basis set superposition error (BSSE) was estimated by following the a posteriori method proposed by Lendvay and Mayer.[71] From the computed binding energies (BE), the BSSE corrected binding energies (BE^c) are obtained as BE^c = BE − BSSE.

3. Experimental Results

3.1. Vibrational Spectroscopies. TS-1 and the parent Ti-free silicalite, synthesized following the patent,[1] are rather defective materials, showing a high density of missing T atoms and so hosting internal hydroxylated cavities[13,19,25,27,32,35−37,54−56] (named nests). The presence of internal SiOH (and possibly TiOH) groups, mutually interacting via a H-bond, makes the IR spectroscopy of H_2O and NH_3 dosed on TS-1 a rather complex matter. In fact, in the same spectral region the following stretching modes overlap: (i) water or ammonia molecules in the liquidlike phase; (ii) water or ammonia molecules adsorbed on Ti(IV) sites or on hydroxyl groups; (iii) SiOH (TiOH) groups interacting with adsorbed molecules and/or with adjacent silanols (titanols).

The interaction with water (Figure 2) and ammonia (Figure 3) molecules has basically a similar effect and will thus be discussed together. Parts a of both figures report the IR spectra of activated TS-1 (dotted spectrum) and after subsequent dosage of increasing P_{H_2O} (dashed and full spectra) and P_{NH_3} (full spectra) in the 3800−1300 cm^{-1} region. This wide spectral range can be divided into two main regions, 3800−2500 and 2100−1400 cm^{-1}, hereafter labeled as regions 1 and 2, respectively. In region 1 the ν(OH) and ν(NH) stretching modes are observed. This region can be further divided into two subregions: 3800−3650 cm^{-1}, including the stretching modes of unperturbed or weakly perturbed OH groups and 3650−2500 cm^{-1}, including the stretching modes of medium-intensity hydrogen-bonded OH groups and the ν(NH) modes of the ammonia molecule.[18,54,56,72,73] Region 2 contains some absorptions due to harmonics and a combination of lower frequency framework modes. In this region, the bending mode δ of the water molecule also occurs at 1634 cm^{-1}. Below 1300 cm^{-1}, down to 750 cm^{-1}, the IR

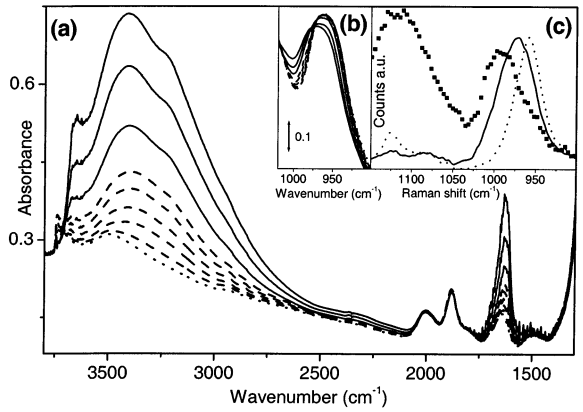

Figure 2. (a) IR spectra, in the 3800−1300 cm^{-1} range, of activated TS-1 (dotted line), and in equilibrium with increasing doses of adsorbed water: low P_{H_2O} (dashed lines) high P_{H_2O} (solid lines). (b) As in (a) in the 1120−901 cm^{-1} range. (c) Raman spectra (λ = 1064 nm) of activated TS-1 (dotted line) and in the presence of a high P_{H_2O} (solid line). The short-dot line spectrum reports the Raman (λ = 244 nm) spectrum obtained by dosing H_2O on TS-1 from the liquid phase (due to the different exciting λ, the increase of the component at 1125 cm^{-1} is not significative–Ref52149400). At low P_{H_2O} (dashed spectra), water interacts mainly with defective silanols, the 960 cm^{-1} band being basically unperturbed, the direct interaction with Ti centers starts at higher P_{H_2O} only (solid spectra).

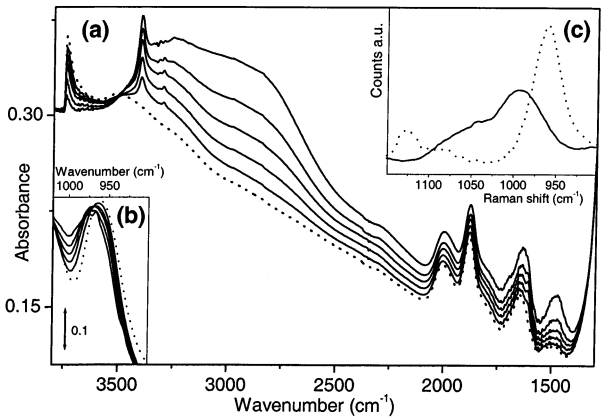

Figure 3. As Figure 2 for the interaction of TS-1 with ammonia. Dashed spectra are absent because NH_3 interacts directly with Ti centers even at the lowest P_{NH_3}.

spectra of TS-1 are totally obscured by the extremely strong ν(Si−O) absorption, with the only exception of a window in the 1000−850 cm^{-1} partially reported in Figures 2b and 3b. In this region TS-1 is characterized by a peculiar, well-defined, band at 960 cm^{-1} (not present in perfect silicalite). This band was immediately considered as a fingerprint of the insertion of Ti atoms in the zeolitic framework[1,17] and tentatively explained in terms of a mode with prevailing Si−O character perturbed by an adjacent framework Ti center.[17,19,20,27,36,37] More recently, a combined cluster and periodical study[25] assigns the 960 cm^{-1} band to the asymmetric stretching of the TiO_4 unit, which can equivalently be described as the out-of-phase antisymmetric stretching of the four connected Ti−O−Si oscillators, or as the out-of-phase stretching of the four Si−O bonds pointing toward Ti. We will return on the 960 cm^{-1} band in great detail in section 4 where theoretical calculation will allow us to confirm the interpretation of ref 25 and to explain the behavior undergone upon interaction with adsorbates (vide infra).

Before dosage of adsorbates, the IR spectrum of TS-1 is characterized by a sharp peak at 3739 cm^{-1} due to external

silanols (titanols) with a shoulder around 3690 cm^{-1} attributed to weakly perturbed silanols (probably due to terminal species in a silanol chain) and by a broad band centered at 3500 cm^{-1} due to internal SiOH (TiOH) groups interacting among themselves in the nests.[18,54,56] In region 2 four zeolite modes appear at 2000, 1880, 1640, and 1490 cm^{-1}.

The interaction with water (ammonia) strongly influences the ν(O−H) modes of TS-1, as shown in Figures 2a and 3a, respectively. Coming to the details of the spectral evolution upon increasing the equilibrium pressure, the first difference between the two experiments appears. Water interacts first with free and with weakly perturbed silanols (titanols) mainly (peak at 3739 cm^{-1} and shoulder around 3690 cm^{-1}). This interaction gives rise to hydrogen-bonded SiOH···OH_2 (TiOH···OH_2) adducts absorbing in the 3400−3150 cm^{-1} range, a phenomenon accompanied by the isosbestic point at 3710 cm^{-1}. The erosion of the 3739 and 3690 cm^{-1} components is progressive, being complete only once the highest P_{H_2O} have been reached. Under these circumstances, water molecules already behave as a liquidlike phase (without any site-specific interaction) confined inside the zeolite channels, as witnessed by a ν(O−H) mode typical of nearly unperturbed H_2O molecules. This band is already visible in the third spectrum (centered at 3685 cm^{-1}) and progressively undergoes a bathochromic shift down to 3645 cm^{-1} upon increasing P_{H_2O}, reflecting the progressive building up of H_2O···H_2O interaction in the liquidlike phase. At the highest P_{H_2O} the spectra are dominated by the vibrational feature of liquidlike water: bands at 3645 and 3410 cm^{-1} and a shoulder around 3230 cm^{-1}, absorbing down to 2900 cm^{-1}. These spectroscopic manifestations well agrees with the heat of adsorption close to the water liquefaction enthalpy reported in the microcalorimetric study (vide infra section 3.3).

The growing of the strong and broad absorption in the 3680−2900 cm^{-1} interval, described above, totally overshadows the much weaker band centered at 3500 cm^{-1} due to internal hydroxyl nests of dehydrated TS-1 (dotted curve). This implies that we are unable to predict if, and at which P_{H_2O}, the adsorbed water molecules begin to interact with SiOH and TiOH groups of the defective nests.

Coming to the discussion of the evolution of the 960 cm^{-1} band, it is worth noticing that the first five water dosages (dashed spectra) do not affect the Ti-specific band either in position or in intensity (Figure 2b). This observation suggests either that interaction with silanols is favored at low P_{H_2O} or that the formation of a Ti(IV)···OH_2 adduct is not able to cause a significant perturbation the 960 cm^{-1} band, which occurs only at higher pressures when more than one water molecule is adsorbed per Ti site. In this regard, quantum chemical calculations (vide infra section 4) will help the interpretation of the experimental results. At higher P_{H_2O}, (full line spectra), when the manifestation of the liquidlike features are already observed, the Ti-specific band progressively shifts at higher frequency up to 971 cm^{-1}, in the highest P_{H_2O} investigated in this experiment.

Figure 2c reports the same experiment followed by Raman spectroscopy (dotted line anhydrous TS-1, solid line highest P_{H_2O}). Also in this case the Ti-specific band undergoes a hypsochromic shift upon contact with water (high P_{H_2O}), moving from 959 to 973 cm^{-1}. Moreover, the strong ν(Si−O) IR absorption in the 1300−1000 cm^{-1} concerns modes that are Raman inactive. This peculiarity allows us to measure the new Ti-specific band at 1125 cm^{-1}.[19,20,24,25] If the experiment is performed by dosing water directly from the liquid phase, the 960 cm^{-1} band undergoes a further shift up to 990 cm^{-1} (see short dashed curve in Figure 2c).[25]

We have thus learnt that the interaction of water (dosed from the gas phase) is extremely weak, but the progressive addition of successive water molecules (highest P_{H_2O} and direct contact with the liquid phase) has a cooperative effect inducing a higher perturbation of the Ti environment.

Coming now to the interaction with NH_3, Figure 3a shows the complete erosion of all the O−H modes of anhydrous TS-1 (sharp peak at 3739 cm^{-1}, shoulder around 3690 cm^{-1} and broad band at 3500 cm^{-1}) accompanied by the parallel growth of a broad band in the 3400−2500 cm^{-1} interval upon increasing P_{NH_3}. This indicates that, in the case of ammonia, the 3500 cm^{-1} band is completely eroded, implying that all silanol (titanol) groups are involved in the interaction with the probe and that the SiOH···NH_3 (TiOH···NH_3) hydrogen bonds are stronger than SiOH···OHSi (SiOH···OHTi) hydrogen bonds responsible for the band at 3500 cm^{-1} in the dotted line spectrum. If comparison is made with the same experiment performed with water (Figure 2a), in the case of ammonia, the broad band due to hydrogen-bonded complexes appears in a definitively lower frequency region (3400−2500 cm^{-1} versus 3600−2900 cm^{-1}), reflecting that NH_3 is a stronger base than H_2O.[72]

The prominent peak at 3399 cm^{-1} is due to the asymmetrical stretching modes of NH_3 perturbed by interaction with the adsorbing silanols, titanols, and Ti(IV) sites (the $\nu_{asym}(NH_3)$ frequency of the free molecule being at 3444 cm^{-1}). The exact location of the less intense band due to the symmetrical stretching modes of NH_3 is not so straightforward due to the presence of Fermi resonances with bending modes;[73] however, it is reasonably assigned to the weak peak observed at 3299 cm^{-1} (the $\nu_{sym}(NH_3)$ frequency of the free molecule being at 3336 cm^{-1}).

As was the case for water, the adsorption of ammonia affects also the intensity and the spectral position of the 960 cm^{-1} band; in fact, a clear upward shift of the maximum of the band is observed upon NH_3 dosage, as shown in Figure 3b (IR) and 3c (Raman). However, in this case, NH_3 interacts directly with Ti even at the lowest P_{NH_3}, reflecting a much higher affinity toward Ti with respect to water. This affinity is also confirmed by the absence of any feature ascribable to liquidlike ammonia such as the sharp δ(NH) component at 1628 cm^{-1}, clearly observed when ammonia is dosed on Ti-free silicalite.[56b]

Comparison with the same experiments performed on Ti-free silicalite (not reported for brevity) is of interest, particularly as a support of the microcalorimetric study where the adsorption isotherms and the heats of adsorption of water and ammonia are reported for both TS-1 and silicalite systems. IR spectra of H_2O dosed on TS-1 (Figure 2a) and on silicalite (not reported for brevity) are basically the same in the whole O−H stretching region, both dominated at the highest P_{H_2O} by the peculiarities of liquidlike water. In contrast, liquidlike ammonia is observed on silicalite only.

3.2. UV−Vis Spectroscopy. On a historical ground, UV−vis spectroscopy has played a key role in the elucidation of the structure of Ti(IV) species in TS-1, both in vacuo and in the presence of adsorbates or in the presence of water or in diluted water solutions of different molecules.[21,25,27,32,33,74−78] The UV−vis spectra of TS-1 in vacuo give a simple and clear proof of the presence of tetrahedral Ti(IV) in the zeolite framework: in fact, a $Ti^{4+}O^{2-} \rightarrow Ti^{3+}O^{-}$ ligand to metal charge transfer (LMCT) located at ≈48 000 cm^{-1} has been assigned to the charge transfer transition from the oxygen ligand to an unoccupied orbital of a Ti(IV) ion tetrahedrally coordinated in the isolated [TiO_4] site.

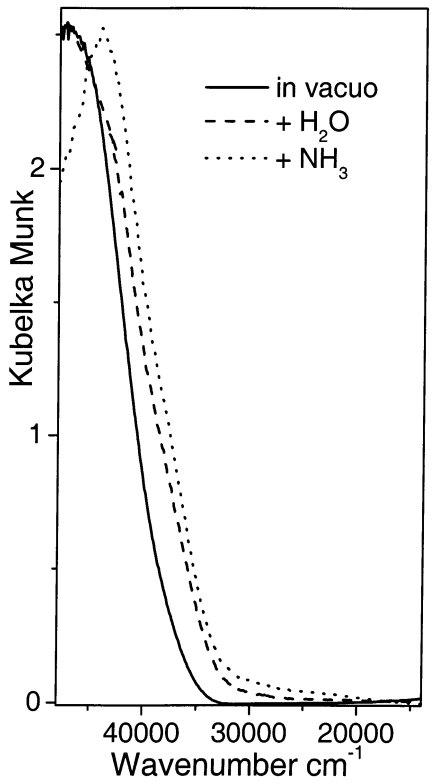

Figure 4. UV−vis spectra of TS-1 catalyst in vacuo (full line) and upon interaction from the gas phase with H_2O (dashed line) and NH_3 (dotted line).

The modification undergone by the UV−vis spectra of TS-1 catalyst in vacuo upon interaction with H_2O and NH_3 (both dosed from the gas phase) is reported in Figure 4. The full line spectrum (dehydrated catalyst) reports, as a unique feature, the LMCT at 48 000 cm^{-1}. Interaction with water (dashed line spectrum) slightly modifies the UV−vis spectrum of TS-1, causing a red shift of the edge, expected as a consequence of the increase of the coordination sphere around Ti(IV) centers.[27] Note, in fact, that in TiO_2, where Ti exhibits six oxygen atoms in its first coordination shell, the $Ti^{4+}O^{2-} \rightarrow Ti^{3+}O^{-}$ LMCT occurs around 32 000 cm^{-1}. A stronger perturbation is obtained upon dosing NH_3 (dotted line curve), but the line shape of the UV−vis curve still remains of the same type (one single maximum).[77]

3.3. Adsorption Microcalorimetry. In Figure 5 the volumetric (section a) and the calorimetric (section b) isotherms of H_2O reversibly adsorbed (second run) on TS-1 and on silicalite are reported. The adsorbed amounts and the integral heats evolved are very close for the two systems, and it is not possible to find a specific interaction between H_2O and Ti(IV) centers. Up to $P_{H_2O} < 3$ Torr, the TS-1 curves are even lower than the ones for silicalite, the difference being, however, within the experimental error. At higher P_{H_2O}, the curves of TS-1 start increasing more rapidly than those of silicalite, suggesting that the interaction between H_2O and Ti(IV) is favored at higher P_{H_2O}, in agreement with the IR evidence. Table 1 reports the quantitative and energetic data taken at low ($P_{H_2O} = 0.5$ Torr) and high ($P_{H_2O} = 5$ Torr) pressure. For each pressure, the energetic data are reported either as integral heat evolved at a given P_{H_2O}, or as mean molar heats normalized to the adsorbed amounts, i.e., $q_p = (Q^{int}/n_{ads})_p$. These latter data refer to the mean adsorption enthalpy ($\Delta_{ads}H$) at the specified P_{H_2O}, which can be taken as a measure of the average energy of interaction of the probe with the active sites: in the present case silanol,

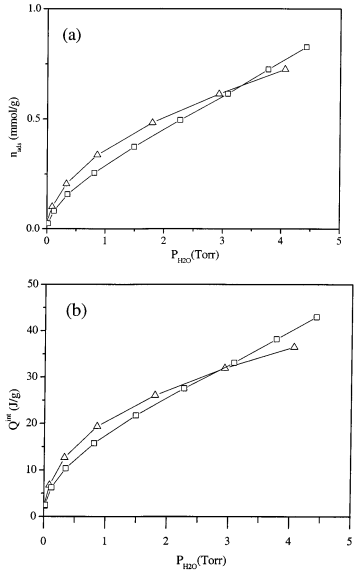

Figure 5. (a) Volumetric isotherms of H_2O reversibly adsorbed (second run) on TS-1 (□) and silicalite (△). (b) Calorimetric isotherms of the samples of (a).

titanol groups, and Ti(IV) centers. The small differences between TS-1 and silicalite makes the contribution to the whole interaction of the Ti(IV) centers not detectable. The mean adsorption enthalpy was found slightly higher on TS-1 than on silicalite (63 against 60 kJ/mol at low P_{H_2O}, and 52 against 50 kJ/mol at high P_{H_2O}), but the difference is too little to be significant. Similar values have also been reported by Corma's group on the Ti-β/H_2O system.[78] The small difference obtained at high P_{H_2O} between the two Ti-containing systems (52 and 50 kJ/mol for TS-1 and Ti-β, respectively) and the Ti-free ones (50 and ≈45 kJ/mol for silicalite and pure silica β, respectively) and the closeness among measured values and the liquefaction enthalpy of water ($-\Delta_L H = 44$ kJ/mol under standard conditions) suggests that the main effect measured by both groups is associated with the condensation of water inside the zeolite pores, which just causes a slight increase of $-\Delta_L H$ (the variation of $-\Delta_L H$ being in the 1−8 kJ/mol range).[60] As a summary, the $\Delta_{ads}H$ of the Ti···H_2O complex is probably much lower than the reported average values and not directly detectable from these experiments.

In contrast, in the case of the adsorption of NH_3, both the volumetric and calorimetric isotherms of silicalite lie below those of TS-1 by a significant amount (Figure 6). On this basis, we can try to evaluate the mean adsorption enthalpy ($\Delta_{ads}H = q_p = (Q^{int}/n_{ads})_p$) for the Ti···$NH_3$ adducts using

$$\Delta_{ads}H = [Q^{int}(\text{TS-1}) - Q^{int}(\text{sil})]/[n_{ads}(\text{TS-1}) - n_{ads}(\text{sil})] \quad (2)$$

Using the data reported in Table 1, eq 2 gives $\Delta_{ads}H$ values as high as 77 and 74 kJ/mol for $P_{NH_3} = 10$ and 80 Torr, respectively. These data deserve detailed comments. First of all, the experimentally measured Q^{int} is an average molar value integrated over all the thermal effects occurring upon dosing ammonia on intrinsically heterogeneous real systems. In the case of TS-1, the average nature of the calorimetric datum reflects the heterogeneity of the catalyst, containing both perfect [Ti-$(OSi)_4$] and defective (hydrolyzed) [$TiOH(OSi)_3$] sites, where NH_3 can form Lewis acid−base adducts, together with defective [$SiOH(OSi)_3$] hydroxyl nests where NH_3 forms H-bonded adducts (vide supra section 3.1). To single out the specific Ti··· NH_3 contribution to the overall Q^{int}, the subtraction between

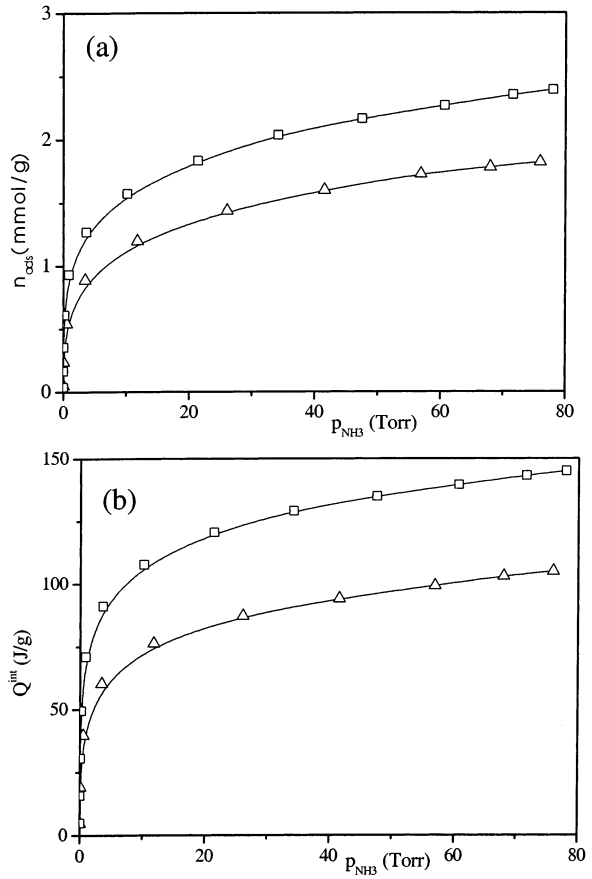

Figure 6. Volumetric isotherms of NH_3 reversibly adsorbed (second run) on TS-1 (□) and silicalite (△). (b) Calorimetric isotherms of the samples of (a).

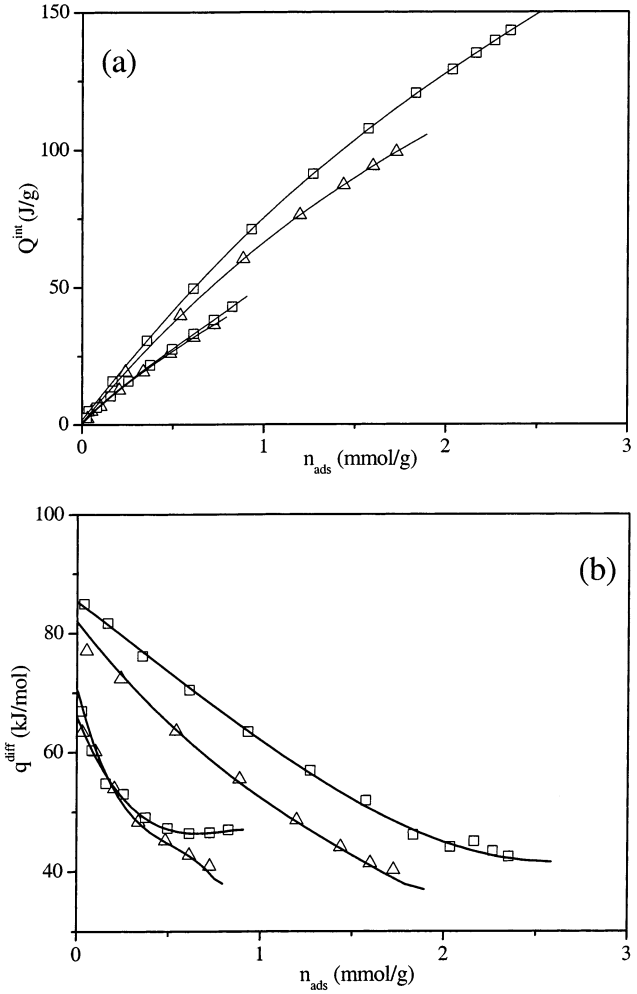

Figure 7. (a) Integral heats evolved during the reversible adsorption (second run) of NH_3 (top side curves) and of H_2O (bottom side curves) on TS-1 (□) and silicalite (△), as a function of the adsorbed amounts. The curves have been interpolated by a polynomial fit of order 4. (b) Differential heat of adsorption ($q^{diff} = -\Delta_{ads}H$) of NH_3 (top side curves) and of H_2O (bottom side curves) as a function of the adsorbed amounts on the samples described in (a). The curves are the derivatives of the polynomials interpolating the integral heat curves as described in (a).

the values obtained on TS-1 and on silicalite should be done [Q^{int}(TS-1) − Q^{int}(sil)], on the basis of the rough assumption that the adsorption of ammonia on silicalite matrix gives the same contribution to Q^{int} at any P_{NH_3} in the two systems. Second, following eq 2, to obtain an estimation of $\Delta_{ads}H$, we must, in the same way, also separate the fraction of NH_3 moles adsorbed on the Ti centers from that adsorbed on the siliceous matrix [n_{ads}(TS-1) − n_{ads}(sil)], the latter being assumed to be unaffected by the presence of Ti. The correct evaluation of both differences is, however, very critical, because studies performed on a set of TS-1 samples characterized by different Ti loading, have shown that the density of internal hydroxyl nests is strongly determined by Ti loading.[13,25,35−37,55,56] Furthermore, a recent HRTEM study has demonstrated that the Ti loading also affects the crystal size and shape of TS-1, so affecting the internal/external surface area ratio of the material.[79] Finally, we have also shown that silicalites synthesized in different ways exhibit a markedly different amounts of internal defects[54−56] and thus show different adsorption isotherms for ammonia.[80] Taken together, these considerations strongly suggest that both Q^{int} and n_{ads} values related to the siliceous matrix of TS-1 cannot be exactly the same as those measured on silicalite. We can so conclude this discussion by stressing that the insertion of Ti atoms in the MFI frameworks significantly increases the ability of the silicalite to adsorb ammonia; however, due to the lack of a "true" blank Ti-free material, the contribution of Ti(IV) species to the overall adsorption cannot be singled out confidentially.

The same conclusions still hold also after a careful analysis of the evolution of the adsorption enthalpy with the increasing coverage, as reported in Figure 7a. In fact, it is immediately evident that in the case of H_2O the curves for TS-1 and silicalite are virtually coincident, whereas in the case of NH_3 the curve for TS-1 lies well above that of the Ti-free matrix, confirming

TABLE 1: RT Reversible Adsorption of H_2O_{vap} and NH_3 (Both Second Run) on TS-1 and Silicalite: Quantitative and Energetic Data at Low (0.5 Torr for Water and 10 Torr for Ammonia) and High (5 Torr for Water and 80 Torr for Ammonia) Equilibrium Pressure

sample/molecule	$(n_{ads})_{lowP}$ (mmol/g)	$(Q^{int})_{lowP}$ (J/g)	$q_{lowP} = (Q^{int}/n_{ads})$ (kJ/mol)	$(n_{ads})_{highP}$ (mmol/g)	$(Q^{int})_{highP}$ (J/g)	$q_{highP} = (Q^{int}/n_{ads})$ (kJ/mol)
TS-1/H_2O	0.19	12.1	63	0.76	39.8	52
silicalite/H_2O	0.25	14.8	60	0.72	36.1	50
TS-1/NH_3	1.54	105.0	68	2.40	146.0	61
silicalite/NH_3	1.11	72.0	65	1.86	105.6	57

TABLE 2: Geometrical Features of the $Ti(OSi)_4$ Moieties in the Different Optimized Bare Clusters (See Figure 1)[a]

model	Ti−O (Å)	α (deg)	β (deg)	Ti−CM (Å)	Ti−O−Si (deg)	Ti−Si (Å)
T5	1.803	109.5	109.5	0.601	180	3.461
CHA_T8	1.809−1.812	108.6−113.8	105.2−110.1	0.562	148.6, 148.7, 152.9, 153.0	3.330−3.367
MFI_T16	1.797−1.813	110.5−111.3	106.4−109.4	0.559	146.2, 151.3, 168.6, 169.5	3.306−3.426
EXAFS	1.79−1.81 ± 0.01				(143, 143, 162, 162) ± 5	3.26−3.38 ± 0.02

[a] Experimental EXAFS data are obtained from ref 35.

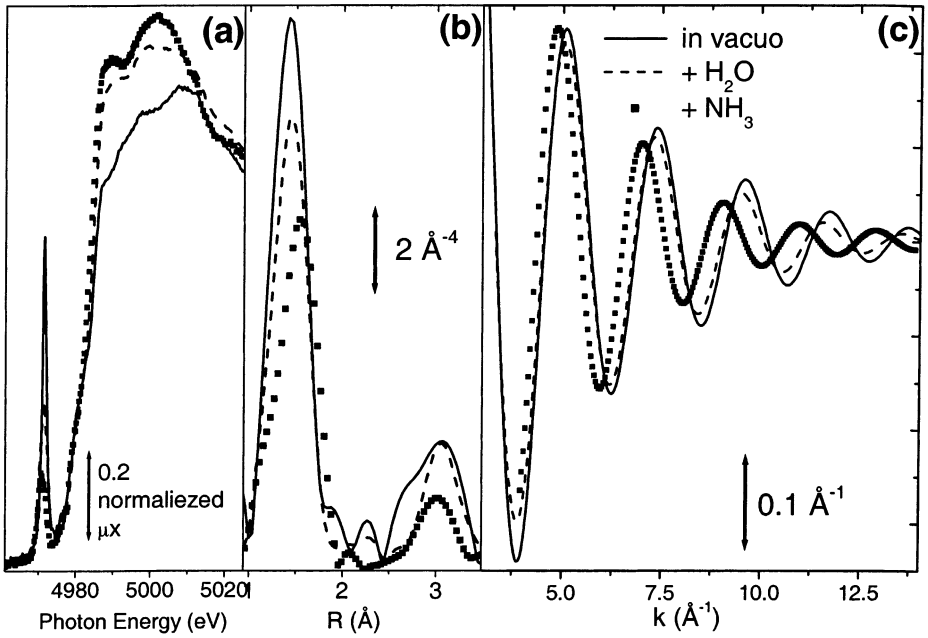

Figure 8. XANES region, k^3-weighted Fourier transformed of the raw EXAFS functions and the corresponding first shell filtered, Fourier back transform (parts a−c, respectively) of TS-1 activated at 400 °C (full lines), after interaction with water (wet sample, dashed lines), and after interaction with NH_3 (P_{NH_3} = 50 Torr, dotted lines).

that a more energetic interaction occurs when Ti(IV) sites are present in the system. In section b of Figure 7, the derivative of the interpolated integral heat curves are reported as well (differential heats of adsorption). In the case of NH_3 the curve for TS-1 lies above that of silicalite in the whole examined interval, suggesting that the Ti(IV) species interact with NH_3 since the early stage of the process. In contrast, in the case of H_2O no specific interaction of Ti(IV) can be singled out. The microcalorimentric data well agree with the different ability of the two probes to perturb the 960 cm^{-1} component as a function of the equilibrium pressure.

3.4. X-ray Absorption Spectroscopies. XANES spectroscopy shows that a narrow and intense preedge peak at 4967 eV due to the 1s → 3d electronic transition involving Ti atoms in tetrahedral coordination is present in well manufactured TS-1[25,27−29,31,33,34,36−38] (full line in Figure 8a). This peak is virtually absent in the case of Ti(IV) octahedrally coordinated. Indeed, the transitions $A_{1g} \rightarrow T_{2g}$ are forbidden for symmetry reasons in the case of octahedral coordination of Ti(IV), but the transition $A_1 \rightarrow T_2$ is allowed in the case of tetrahedral-like coordination of Ti(IV), as $[TiO_4]$ units of TS-1.

Interaction with H_2O (liquid drop on the sample) and with NH_3 (from the gas phase) implies a reduction of the 4967 eV preedge peak accompanied by an increase of the white line (first resonance after the edge) intensity, witnessing the insertion of ligand molecules in the coordination shell of Ti(IV) and a modification of the local geometry from a tetrahedral to a nearly tetrahedral one. The perturbation of the XANES region (Figure 8a) induced by wetting the sample is smaller than that induced by interaction with NH_3 from the gas phase. The same holds for the radial distribution around Ti (Figure 8b). The modification of the second shell contribution in the 2.5−3.5 Å range is also noticeable. Moreover, if we compare, for the two cases, the first shell filtered Fourier back transform functions (Figure 9c), we see that the interaction with H_2O causes only a very small decrement of the oscillations period, witnessing a small elongation of the four Ti−O bonds needed to accommodate the water molecules in the coordination sphere of Ti, and a much

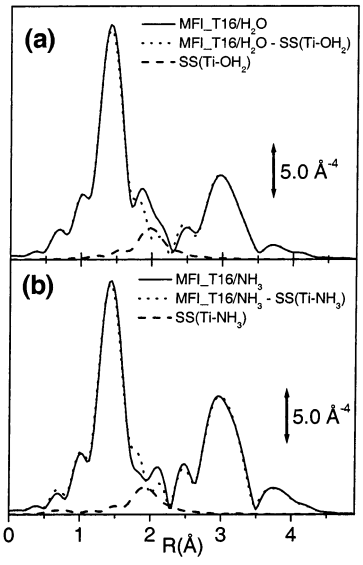

Figure 9. (a) FEFF8 simulation of the MFI_T16/H_2O cluster (full line), of the single scattering Ti−OH_2 contribution (dashed line), and of the MFI_T16/H_2O cluster without the Ti−OH_2 path (dotted line). (b) As in (a) for the MFI_T16/NH_3 cluster.

TABLE 3: Geometrical and Energetic Features of the $Ti(OSi)_4$ Moieties in the Different Optimized Clusters upon Adsorption of H_2O and NH_3 Molecules (L = OH_2 and NH_3, Respectively)

model	Ti−O (Å)	Δ⟨Ti−O⟩ (Å)	α (deg)	β (deg)	Ti−CM (Å)	Ti−O−Si (deg)	Ti−Si (Å)	Ti−L (Å)	BE (kJ mol^{-1})	BE[c] (kJ mol^{-1})
T5/H_2O	1.804−1.841	+0.020	116.1−116.6	100.7−102.1	0.356	151.4, 152.0, 168.3, 170.1	3.390−3.449	2.43	12.0	2.1
CHA_T8/H_2O	1.807−1.850	+0.019	113.8−119.0	99.1−101.6	0.337	145.2, 152.3, 154.7, 160.5	3.332−3.406	2.40	25.0	13.7
MFI_T16/H_2O	1.807−1.845	+0.019	115.4−117.0	99.9−101.8	0.351	147.1, 151.8, 161.1, 174.0	3.338−3.436	2.41	29.7	15.4
T5/NH_3	1.822−1.836	+0.029	117.5−117.9	98.8−98.9	0.282	155.3, 155.3, 156.0, 179.4	3.407−3.472	2.35	26.4	17.4
CHA_T8/NH_3	1.835−1.844	+0.029	114.9−119.9	97.6−99.6	0.270	143.7, 145.0, 159.6, 160.8	3.311−3.427	2.33	42.9	32.8
MFI_T16/NH_3	1.829−1.840	+0.027	117.0−118.2	98.1−99.8	0.292	150.7, 156.5, 167.9, 178.4	3.360−3.457	2.35	45.5	33.0

TABLE 4: Filtering Ranges and EXAFS Results for First Coordination Sphere of the TS-1 Sample in Vacuo (One Shell Fit) and after Interaction with Water (One Shell Fit) and with 60 Torr of Ammonia (Two and One Shell for Models I and II, Respectively: See Text)[a]

sample conditions	Δ*k* (Å^{-1})	Δ*R* (Å)	shell	*R* (Å)	*N*	$10^2\sigma$ (Å)	Δ*E* (eV)
in vacuo	3.34−14.31	1.07−1.84	Ti−O	1.79 ± 0.01	4.30 ± 0.25	5.5 ± 0.6	−2.0 ± 1.1
+H_2O			Ti−O	1.82 ± 0.02	4	5.8 ± 0.7	−3.0 ± 1.3
+NH_3	2.93−14.09	0.96−1.96	Ti−O	1.84 ± 0.03	4	9 ± 2	−4 ± 4
model I +NH_3			Ti−N	1.93 ± 0.04	1.9 ± 0.4	6 ± 2	+5 ± 4
model II	2.93−14.09	0.96−1.96	Ti−O	1.88 ± 0.02	4	7.6 ± 1.0	0 ± 2

[a] Δ*k*, interval of *k*-space to *R*-space FT; Δ*R*, *R*-space interval selected to perform the first shell-filtered back FT into *k*-space; *R*, bond distance; *N*, coordination number; σ, relative Debye−Waller factor; Δ*E*, energy shifts. Nonoptimized parameters can be discriminated by the absence of the corresponding error bars.

greater effect caused by ammonia. The results are in qualitative agreement with IR, UV−vis, and calorimetric data (vide supra sections 3.1., 3.2, and 3.3, respectively).

The structural parameters determined in the EXAFS data analysis on the sample in vacuo and after interaction with water and ammonia will be reported in section 4, once ab initio studies have provided a model on the formation of Ti(IV)···OH_2 and Ti(IV)···NH_3 adducts (vide infra Table 4).

4. Computational Results and Discussion

4.1. Geometrical Features in the Bare Clusters. The optimized structures of clusters T5, CHA_T8, and MFI_T16 are reported in Figure 1a,c,e, respetively (vide supra section 2.3), and the main geometrical parameters have been summarized in Table 2. Cluster T5 has both first and second shells around Ti in a nearly perfect T_d symmetry (α = β = 109.5°), which is broken by the zeolitic framework constraints in models CHA_T8 (where the six α and β angles[81] lie in the 108.6−113.8° and 105.2−110.2° intervals, respectively) and MFI_T16 (110.5° < α < 111.3° and 106.4° < β <109.4°).

The T_d symmetry of model T5 results in a unique first shell Ti−O distance at 1.803 Å, whereas model CHA_T8 exhibits two distances at 1.809 and 1.812 Å and model MFI_T16 shows four different distances in the 1.797−1.813 Å range. These values well agree with EXAFS experimental data, reporting the Ti−O distance in the 1.79−1.81 Å interval[27−37] (with a typical error of ±0.01 Å), and with previous theoretical studies on the $Ti(OSiH_3)_4$ cluster[51,53,65,66] (1.798−1.830 Å range).

Coming to the higher shells, model T5 shows four linear equivalent Ti−O−Si moieties, whereas distortions are present in the CHA_T8 and MFI_T16 models where two couples of Ti−O−Si angles are present. In model CHA_T8, the two couples are rather close, differing only about 4° (see Table 2), and in model MFI_T16, they are significantly different (21°), the narrower one occurring around 148° and the larger one around 169°. On the experimental ground, the fit of the overall EXAFS signal (containing both first and second shell contributions) improves significantly by moving from a model containing a single Ti−O−Si contribution to a model containing two independent Ti−O−Si contributions.[35] Under such conditions the two independent Ti−O−Si angles have been optimized to 143 ± 5° and 162 ± 5°, in rather close agreement with the values obtained from model MFI_T16. Furthermore, a satisfactory agreement is obtained for the two couples of Ti−Si distances: 3.26 ± 0.02 and 3.38 ± 0.02 Å (experimental) and 3.306−3.426 Å (model MFI_T16). Also, model CHA_T8 gives reasonable Ti−Si distances (3.330−3.367); however, it is not able to reproduce the splitting between short (narrow) and long (large) distances (Ti−O−Si angles). These results, mimicking a portion of the chabazite framework, can be compared with those obtained by Zicovich-Wilson et al.[48] who studied Ti−chabazite (Si/Ti = 1:1) using a periodical approach with the CRYSTAL[82] code. They found Ti−O distances, Ti−O−Si angles, and Ti−Si distances in the 1.78−1.79 Å, 150−157°, and 3.28−3.34 Å ranges, respectively. Less satisfactory results are obtained with model T5, giving a definitively too long Ti−Si distance (caused by Ti−O−Si = 180°; see Table 2).

On the basis of this preliminary study on the bare clusters, it emerges that the second shell around Ti(IV) is correctly reproduced only after insertion of the $[Ti(OSi)_4]$ unit inside bigger clusters mimicking the zeolitic framework.

4.2. Perturbation of the Geometrical Features upon H_2O and NH_3 Adsorption. As EXAFS told us that also the second shell of the $[Ti(OSi)_4]$ unit is involved in the adsorption process (see Figure 8b) the data coming from models CHA_T8 and MFI_T16 are the most reliable. Corresponding data coming from model T5 are reported for comparison only.

The first evidence of our calculation on all clusters is that the adsorption of both molecules causes an increase of the first shell Ti−O distances (Table 3 vs Table 2). The Δ⟨Ti−O⟩, averaged on the four bonds, are +0.02 and +0.03 Å for H_2O and NH_3 molecules, respectively. This datum is in qualitative

agreement with the first shell EXAFS data, obtained under conditions where more than one ligand molecule is adsorbed on Ti(IV) sites (see Table 4) reporting $\Delta\langle Ti-O\rangle = +0.03$ Å (for H_2O) and +0.05 Å (for NH_3, model I, see refs 36 and 37). In all cases we observe that ligand absorption causes a (further) distortion from tetrahedral toward bipiramidal symmetry, as monitored by the modification of α and β angles (see bottom of Figure 1), which tend to 120 and 90°, respectively. In all clusters, NH_3 is slightly more efficient in the distortion of the T_d symmetry. This fact agrees well with the IR evidence showing that NH_3 is more efficient than H_2O in the perturbation of the 960 cm^{-1} band (particularly when low equilibrium pressures are concerned, see section 3.1). The same holds for the reduction of the 4967 eV preedge peak in XANES spectra (see section 3.4). Ligand adsorption also modifies the second shell environment, as documented by the Ti−O−Si and Ti−Si columns in Table 3. No multiple scattering second shell fit of TS-1 in interaction with H_2O and NH_3 is available up to now; so quantitative comparison between theoretical and experimental data is not feasible.[83] However, even from a simple view of the raw FT of the experimental EXAFS data (Figure 8b) the modification of the second shell signal is evident.

Coming to the equilibrium distance of the ligand molecules (Ti−L, L = H_2O, NH_3) all clusters gives a definitively shorter Ti−L in the case of ammonia (≈2.34 vs ≈2.41 Å; see Table 3), reflecting the stronger interaction. The results obtained on the TS-1/H_2O system are compatible with the EXAFS data. In fact, a Ti···OH_2 distance of 2.41 Å should be above the first shell peak due to Ti−O contributions and thus will not affect the first shell data analysis reported in Table 4. On the basis of the computed Ti···OH_2 distance of 2.41 Å the contribution of adsorbed molecules would be expected in the R region between the first Ti−O and second Ti−Si shell peaks reported in Figure 8b. Some features are effectively present upon water adsorption in the 1.90−2.65 Å (phase uncorrected) interval; however their low intensity prevents any attempt to obtain reliable structural data. This experimental datum could be interpreted only on the basis of a high Debye−Waller factor of the Ti···OH_2 bond, suggested by the very low bonding energies also evidenced by the microcalorimetric data (Table 1) and computed by ab initio methods (Table 3). On this basis, adsorbed water molecules are not directly detected by EXAFS, which is only able to measure the effect that the H_2O adsorption has on the Ti−O bond lengths. This hypothesis will be further confirmed by the simulation of the EXAFS signal of the MFI_T16/H_2O clusters performed in the frame of the multiple scattering approach (vide infra at the end of this section). Corma and co-workers[78] reported a two-shell EXAFS fit for rehydrated Ti-β samples. In that work, the first shell simulates the contribution of the four framework oxygen atoms and the second simulates the oxygen of the adsorbed water molecules, resulting in Ti···OH_2 distances in the 2.12−2.20 Å interval. The authors, however, stress that, due to the high number of optimized parameters, the results of the two-shell fit should be considered with care. They have therefore analyzed the same experimental data using a one-shell fit: in such a model they just observe the increase of the average Ti−O distance of the framework oxygen ($\Delta\langle Ti-O\rangle = 0.03-0.04$ Å). We have adopted here this second approach to analyze the data obtained on TS-1, with comparable results (Table 4).

Similarly, for ammonia a Ti···NH_3 distance of 2.34 Å is expected to give an EXAFS contribution between the first and the second shell peaks. Like discussed for H_2O, such a contribution does not result in an appreciable signal in the experimental EXAFS spectrum reported in Figure 8b (vide infra the simulation of the EXAFS signal done on the MFI_T16/NH_3 cluster). A fit of the EXAFS datum with a very low residual has been obtained in the past (model I in Table 4, see refs 36 and 37) with a model simulating a Ti−O shell of four atoms (framework oxygens) at 1.84 Å and two N atoms (ammonia) at 1.93 Å. This fit must be considered with caution in view of the high difference of the ΔE values obtained for the Ti−O and Ti−N shells (Table 4). Moreover, the Ti−N distances of crystalline compounds where titanium is simultaneously coordinated to four oxygen atoms lie in the 2.38−2.05 interval.[84] On these bases, model I of Table 4 must be critically reconsidered. In fact, a Ti−N distance as short as 1.93 Å should be associated with a very strong Ti···NH_3 interaction enthalpy, which is not supported by the high percentage of reversible adsorption (see section 3.3). According to the ab initio results, showing that the four Ti−O distances differ only by less than 0.03 Å upon NH_3 adsorption (a value well comparable with the EXAFS accuracy), we have refined the experimental data with a single Ti−O shell (model II in Table 4), as done in the case of water adsorption. Model II gives a Ti−O distance of 1.88 Å. This value is larger than that obtained from ab initio computations (1.83−1.84 Å) but has been obtained on EXAFS data performed in the presence of high P_{NH_3}, where more than one ammonia molecule is adsorbed per Ti site (and hence the Ti−O distance is expected to be further relaxed). Model II is thus compatible with ab initio and calorimetric results. It is evident that this point will be definitively clarified only once a complete higher shell fit of the EXAFS data is performed on the basis of the multiple scattering approach.

This study is still in progress and hereafter we will report the preliminary results of a multiple scattering simulation of the EXAFS signal of MFI_T16/H_2O and MFI_T16/NH_3 clusters. These have been optimized with the ONIOM method and are used now as input of the FEFF8 code.[64] The aim of these simulations is to evaluate the weight of the single scattering Ti−OH_2 (Ti−NH_3) contribution to the overall EXAFS signal of TS-1 in interaction with water (ammonia). So no geometrical optimization of the clusters nor of the Debye−Waller factors σ of the different paths has been performed in the FEFF8 simulations, the latter being arbitrarily fixed to $\sigma = 0.0$ for all paths. Under these assumptions, the simulated EXAFS signal is reported in the full line spectra of Figure 9a,b for MFI_T16/H_2O and MFI_T16/NH_3 clusters, respectively. The single scattering Ti−OH_2 (Ti−NH_3) contribution is reported in the dashed line curve in Figure 9a (9b), and the EXAFS signals of MFI_T16/H_2O and MFI_T16/NH_3 without the Ti−OH_2 (Ti−NH_3) contribution are reported in the dotted line curves. In both cases, the closeness between the full and dotted line curves is the direct consequence of the low weight that the single scattering Ti−OH_2 (Ti−NH_3) contribution gives to the overall EXAFS signal. Moreover, this simulation has been performed using the same Debye−Waller factors ($\sigma = 0$) for all paths, although it is clear that adsorbed molecules (H_2O and NH_3) must have a much higher σ value than that of the paths involving framework (O and Si) atoms. This means that the actual single scattering Ti−OH_2 (Ti−NH_3) contribution will have an even lower relative weight than that resulting from Figure 9.

Notwithstanding the fact that we are dealing with a zero level simulation, the results reported in Figure 9 are important because they allow us to prove that the modification of the overall EXAFS signal caused by the insertion of a water or an ammonia molecule into the first coordination shell of Ti(IV), is due to the modification of the framework O and Si position to accommodate the ligand molecule and not to the single

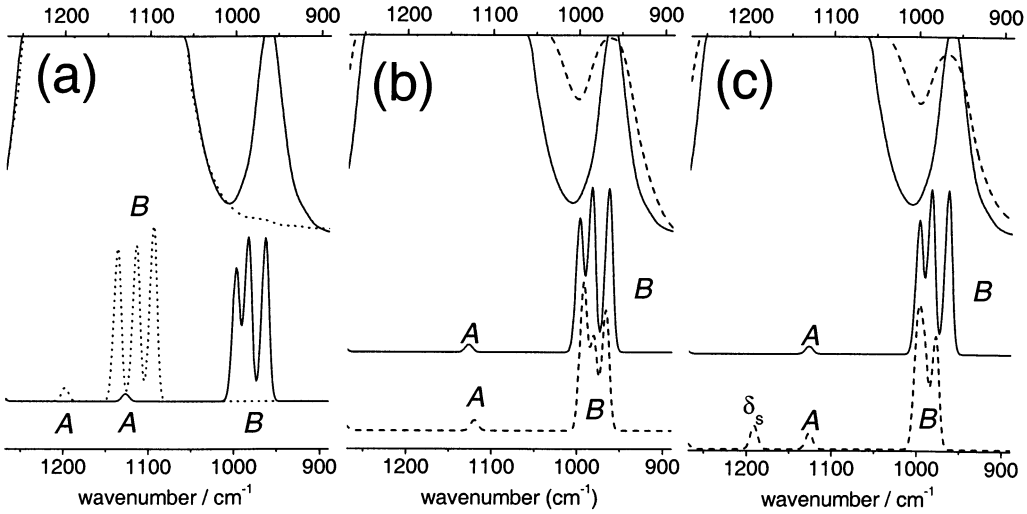

Figure 10. (a) Comparison between experimental (top curves) and computed (bottom curves) IR spectra of dehydrated TS-1 (solid lines) and silicalite (dotted lines). (b) As in (a) for TS-1 before (solid line) and after (dashed line) interaction with water. (c) As in (b) for TS-1 before (solid line) and after (dashed line) interaction with ammonia.

scattering Ti−OH_2 and Ti−NH_3 contribution. This supports the hypothesis in section 4.2.

4.3. Energetics of the H_2O and NH_3 Adsorption. On the energetic ground, for both adsorbed molecules, a remarkable difference is observed by moving from model T5 to the models CHA_T8 and MFI_T16, where the framework constraints are considered (Table 3). The water adduct formed on the T5 cluster is nearly unbounded, the BSSE corrected binding energy (BE^c = BE − BSSE)[71] being only 2.1 kJ mol^{-1}. Even if BE^c increases considerably in models CHA_T8 and MFI_T16 (13.7 and 15.4 kJ mol^{-1}, respectively), we are still dealing with very low values. Comparison with other theoretical results yields the following picture. (a) Ricchiardi et al.,[50] using a hybrid periodic embedded molecular mechanics/quantum mechanics cluster approach as implemented in QMPOT[85] code, obtain BE^c values in the 23−31 kJ mol^{-1} range for three different T sites of TS-1 and a value of 29 kJ mol^{-1} for Ti−chabazite at the Hartree−Fock (HF) level. (b) Zicovich-Wilson et al.[48] reported a BSSE-uncorrected binding energy (BE) of 34.4 kJ mol^{-1} for Ti−chabazite (periodic approach, HF level). (c) Sinclair et al.[47] give a BSSE-uncorrected BE of 12 kJ mol^{-1} for the [$Ti(OSiH_3)_4$] cluster (BP level). (d) Munakata et al.[52] reported a BSSE-uncorrected BE of 41 kJ mol^{-1} for the [$Ti(OSi(OH_3))_4$] cluster (calculated at B−P level on an LDA optimized structure). Even if we observe a consistent spread of the computed BE values, we are always dealing with very weak interactions (below or comparable with the water condensation enthalpy 44 kJ mol^{-1}). This fact qualitatively agrees with the numerous experimental evidences reported above: (i) invariance of the 960 cm^{-1} band in low P_{H_2O} IR spectra, (ii) small perturbation of both XANES and EXAFS spectra, and (iii) calorimetric adsorption isotherms, not distinguishable from that performed on the Ti-free silicalite, reporting q_{ads} values approaching, at high P_{H_2O}, to the condensation enthalpy in both cases.

The BE^c computed for the Ti···NH_3 adducts on all clusters are significantly higher (more than 100%) than the corresponding values obtained for the Ti···OH_2 adducts: 17.4, 32.8, and 33.0 kJ mol^{-1} for models T5, CHA_T8, and MFI_T16, respectively (Table 3). This fact is not unexpected, due to the higher basicity of ammonia, and qualitatively agrees with all the observed differences between the TS-1/H_2O and TS-1/NH_3 systems. Unfortunately, no quantitative comparison is available with experimental data. In fact, though the theoretical model proposed in this study quantifies the interaction between a Lewis center, the [$Ti(OSi)_4$] unit embedded in different clusters, and the basic NH_3 molecule, the experimental data result from the simultaneous contributions coming from the interaction between ammonia and acidic sites of pure Lewis, pure Brønsted, and joint Lewis/Brønsted nature: [$Ti(OSi)_4$], [$SiOH(OSi)_3$], and [$TiOH(OSi)_3$], respectively. A direct quantitative comparison between theoretical and experimental data is so not feasible with confidence owing to the absence of a straightforward method able to separate, at each P_{NH_3}, the measured quantities (Q^{int} and n_{ads}) into the corresponding subquantities referred to the three individual adsorption sites (see section 3.3).

Besides the quantitative specific values, BE^c shows a significant trend for both TS-1/H_2O and TS-1/NH_3 systems, by moving from the unconstrained model T5 to the framework constrained ones (CHA_T8 and MFI_T16). The increase of the BE^c of about 2 (NH_3) and 6 (H_2O) times suggests a higher Lewis acidity of Ti(IV), when the [$Ti(OSi)_4$] moiety is inserted in the zeolitic framework. The origin of this fact is probably related to a reduction of the energetic cost needed to deform the [$Ti(OSi)_4$] unit to allow the insertion of an extra ligand (e.g., H_2O or NH_3). In fact, insertion in the zeolitic framework already induces a partial deformation from perfect T_d symmetry (see Table 2 and related discussion). A detailed discussion on the deformation energy of the [$Ti(OSi)_4$] unit upon insertion in the zeolitic framework is reported elsewhere.[67] This could be one of the possible reasons explaining why Ti species in TS-1 are more reactive than grafted Ti species.

4.4. Vibrational Features in the Bare Clusters. Model MFI_T16 being the more representative for silicalite and TS-1, we will focus the discussion on the vibrational features mainly on it, which has been computed with either Si or Ti as the central atom. In the totally siliceous cluster, the central $Si(OSi)_4$ moiety is characterized by two main vibrational features: a single band centered at 1198 cm^{-1} and a triplet (1138, 1115, and 1095 cm^{-1}), labeled in Figure 10a as components A and B, respectively. Band A (IR, weak) is the totally symmetric combination of the four ν_{asym}(Si−O−Si) modes, whereas feature B (IR, strong, triply degenerated in a perfect T_d symmetry) originates from their asymmetric combinations. The computed IR spectrum covers only a part of the broad experimental

TABLE 5: Vibrational Features (A and B Modes) of Bare and Engaged T5 and MFI_T16 Models for TS-1

model	B $\bar{\nu}_1$ (cm^{-1})	B $\bar{\nu}_2$ (cm^{-1})	B $\bar{\nu}_3$ (cm^{-1})	B $\langle\bar{\nu}\rangle$ (cm^{-1})	A (cm^{-1})
T5	983	$\bar{\nu}_1$	$\bar{\nu}_1$	$\bar{\nu}_1$	1102 (IRNA[a])
T5/NH_3	953	959	960	958.4	1077
MFI_T16	964	984	998	980.9	1127
MFI_T16/H_2O	967	981	993	981.2	1120
MFI_T16/NH_3	978	991	999	989.6	1126

[a] IRNA = IR nonactive.

absorption (upper dotted curve in Figure 10a) due to the heterogeneity of T sites environment in MFI (12 independent T sites), which is supposed to slightly affect the frequencies of A and B modes. The experimental spectrum can so be considered as the sum of 96 A and B features corresponding to the 96 T centers in the orthorhombic MFI unit cell.

Insertion of Ti in the central T site of the cluster strongly perturbs the geometrical features of the local structure (vide supra section 4.1), which in turn reflects on the vibrational features. The B triplet is significantly affected, now being located at 998, 984, and 964 cm^{-1}, i.e., in a region very close to the experimental component centered at 960 cm^{-1} (Figure 10a). Also mode A undergoes a consistent red shift, moving to 1127 cm^{-1}. This band, not visible in the experimental IR spectrum because it appears in the broad 1250−1030 cm^{-1} range (where A and B features of the predominant siliceous part of TS-1 strongly absorb), corresponds to the 1125 cm^{-1} Raman band,[19,20] enhanced when a 244 nm UV laser is used.[24,25]

For the sake of comparison, we shall stress that in the much simpler T5 cluster, the A mode appears at 1102 cm^{-1}, being completely IR inactive, and the B triplet is centered at 983 cm^{-1}, being completely degenerated (Table 5).

4.5. Perturbation of the Vibrational Features upon H_2O and NH_3 Adsorption. A progressive blue shift of the 960 cm^{-1} band has been observed upon increasing the equilibrium pressure of the H_2O and NH_3 probe molecules (see upper curves in Figure 10b,c and vide supra section 3.1). In previous works[17,19,27,36,37] the 960 cm^{-1} band has been intuitively explained in terms of a mode with prevailing Si−O character perturbed by the adjacent framework Ti center. According to this simple model, the interaction of Ti(IV) with an adsorbed molecule will imply a reduction of the perturbation induced on the adjacent Si−O moieties, resulting in the convergence of the 960 cm^{-1} band with the unperturbed ν_{asym}(Si−O−Si) mode adsorbing in the wide 1250−1030 cm^{-1} interval (Figure 10a).

The adsorption of one H_2O molecule affects only slightly the vibrational peculiarities of cluster MFI_T16 (see Table 5 and Figure 10b), the B triplet now being located at 967, 981, and 993 cm^{-1}. Its center of mass is nearly unchanged (+0.3 cm^{-1}) with respect to the bare cluster. This fact agrees with the invariance of the 960 cm^{-1} in the first stages of water adsorption (see section 3.1). Mode A undergoes a red shift of 7 cm^{-1}.

Also, the calculated frequencies on the MFI_T16/NH_3 complex reflect what is experimentally observed, the B triplet being shifted up to 999, 991, and 978 cm^{-1} (Table 5). If comparison is made on the center of mass, it moves from 981 to 990 cm^{-1}, in agreement with the $\Delta\bar{\nu} = 8$ cm^{-1} experimentally observed at low P_{NH_3}. Concerning the A mode, it appears at the same frequency (1126 vs 1127 cm^{-1}), being slightly intensified. Unfortunately, for the A mode, comparison with the experimental shift is not feasible for IR data. The new band at 1191 cm^{-1} (Figure 10c) is the δ_s umbrella mode of NH_3 shifted upward (from the computational value of 1000 cm^{-1}) upon absorption on Ti center.

It is finally worth noticing that the T5 model is not able to predict the correct sign of the shift of the B triplet upon ammonia adsorption, the computed shift being −24.6 cm^{-1} (Table 5). This fact evidences the importance of the zeolitic environment in determining the fine structure of the vibrational modes related to Ti atoms and their modification upon interaction with probes.

5. Conclusions

In this work we report on the effect of H_2O and NH_3 adsorption on the vibrational, electronic, and energetic features of Ti(IV) centers in TS-1 on both experimental and theoretical grounds. Experimental and computational results confirm that ammonia perturbs the local environment of Ti(IV) to a greater extent than water does. In most cases a remarkable agreement between computed and experimentally observed features has been obtained; in particular, the following points are worth noticing. (1) Our computations show that a reliable description of the Ti environment up to the second shell can be obtained only if the zeolitic constraint are included in the model. Under this basis we have reproduced the following structural data (in parentheses the disagreement with experimental values): the first shell Ti−O distance at 1.792 Å (within 0.01 Å); the presence of two couples of Ti−O−Si angles around 148 and 169° (both within 5°); the presence of two couples of second shell Ti−Si distances at 3.306−3.426 Å (both within 0.05 Å). (2) The adsorption of both H_2O and NH_3 molecules caused the stretching of the Ti−O bond in agreement with the experimental values with an error of 0.01 and 0.02 Å with the experimental values. (3) The computed energetic of the formation of the water complexes is low (15.4 kJ mol^{-1}), in agreement with the calorimetric data here reported for the first time. (4) The computed energetic of the formation of the ammonia complexes (33.0 kJ mol^{-1}) has induced us to critically reinterpret previous calorimetric and EXAFS data, resulting in a new picture, where ammonia molecules are less strongly coordinated to Ti(IV) centers than previously claimed.[36,37] (5) We report the first clear computational evidence that the insertion of the Ti[OSi]$_4$ moiety inside a cluster mimicking the zeolitic framework strongly increases the reactivity of the Ti site toward both H_2O and NH_3 probes. (6) We report for the first time the vibrational analysis of titanosilicates based on a model bigger than the Ti(OSiH_3)$_4$ one, which is representative of the MFI framework. As far as the bare cluster is concerned, the computed vibrational frequency for the A mode differs from the experimental one (Raman) by 2 cm^{-1}, whereas the computed center of mass of the B triplet is overestimated by 21 cm^{-1} with respect to the experimental 960 cm^{-1} band observed in IR spectra, which, however, has a full width at half-maximum of 27 cm^{-1}. An even closer agreement is obtained by comparing the calculated blue shifts undergone by the center of mass of the B triplet upon adsorption of one water (ammonia) molecule with the experimental values: $\Delta\langle\bar{\nu}\rangle = +0.3$ and $\Delta\bar{\nu} = 0$ for water and $\Delta\langle\bar{\nu}\rangle = +8.7$ and $\Delta\bar{\nu} = 8$ for ammonia. Notice that the simpler Ti(OSiH_3)$_4$ model, which does not consider the embedding in the MFI framework is unable to give the observed blue shift of the B triplet.

Ab initio calculations have suggested a way to improve the model for simulating the EXAFS data. On computational grounds, future developments will follow three different directions: (i) inclusion of hydroxylated defects in the cluster models, (ii) the study of cooperative effect related to the multiple adsorption on the same site, and (iii) the investigation of long-range interaction with the use of periodic models.

Acknowledgment. This study has been supported by MURST COFIN2000 "*Structure and reactivity of catalytic centers in zeolitic materials*". We acknowledge the Renishaw for the kind access to the UV-Raman instrument (R. Tagliapietra) and for the scientific and technical support during measurements. We thank the BM8 GILDA staff at the ESRF and the EXAFS13 group of LURE (in particular F. D'Acapito and F. Villain), for important scientific and technical support during X-ray absorption measurements. We are indebted to M. Ricci (Polimerieuropa Novara) and P. Ugliengo (University of Turin) for fruitful discussions.

References and Notes

(1) Taramasso, M.; Perego, G.; Notari, B. U.S. Patent No. 4410501, 1983.

(2) Meier, W. M.; Olson, D. H.; Baerlocher, Ch. *Atlas of Zeolite Structure Types*; Elsevier: London, 1996. Thomas, J. M.; Bell, R. G.; Catlow, C. R. A. In *Handbook of Heterogeneous Catalysis*; Ertl, G., Knözinger, H., Weitkamp, J., Eds.; VCH: Weinheim, 1997; p 286−310.

(3) Clerici, G. M. *Appl. Catal.* **1991**, *68*, 249.

(4) Clerici, G. M.; Bellussi, G.; Romano, U. *J. Catal.* **1991**, *129*, 159.

(5) Bellussi, G.; Carati, A.; Clerici, G. M.; Maddinelli, G.; Millini, R. *J. Catal.* **1992**, *133*, 220.

(6) Notari, B. *Adv. Catal.* **1996**, *41*, 253 and references therein.

(7) Roffia, P.; Leofanti, G.; Cesana, A.; Mantegazza, M. A.; Padovan, M.; Petrini, G.; Tonti, S.; Gervasutti, P. *Stud. Surf. Sci. Catal.* **1990**, *55*, 543.

(8) Mantegazza, M. A.; Leofanti, G.; Petrini, G.; Padovan, M.; Zecchina, A.; Bordiga, S. *Stud. Surf. Sci. Catal.* **1994**, *82*, 541.

(9) Mantegazza, M. A.; Petrini, G.; Spanò, G.; Bagatin, R.; Rivetti, F. *J. Mol. Catal. A* **1999**, *146*, 223.

(10) Millini, R.; Previdi Massara, E.; Perego, G.; Bellussi, G. *J. Catal.* **1992**, *137*, 497.

(11) Lamberti, C.; Bordiga, S.; Zecchina, A.; Carati, A.; Fitch, A. N.; Artioli, G.; Petrini, G.; Salvalaggio, M.; Marra, G. L. *J. Catal.* **1999**, *183*, 222.

(12) Marra, G. L.; Artioli, G.; Fitch, A. N.; Milanesio, M.; Lamberti, C. *Micropor. Mesopor. Mater.* **2000**, *40*, 85.

(13) Lamberti, C. Bordiga, S.; Zecchina, A.; Artioli, G.; Marra, G. L.; Spanò, G. *J. Am. Chem. Soc.* **2001**, *123*, 2204.

(14) Henry, P. F.; Weller, M. T.; Wilson, C. C. *J. Phys. Chem. B* **2001**, *105*, 7452.

(15) Hijar, C. A.; Jacubinas, R. M.; Eckert, J.; Henson, N. J.; Hay, P. J.; Ott, K. C. *J. Phys. Chem. B* **2000**, *104*, 12157.

(16) Tozzola, G.; Mantegazza, M. A.; Ranghino, G.; Petrini, G.; Bordiga, S.; Ricchiardi, G.; Lamberti, C.; Zulian, R.; Zecchina, A. *J. Catal.* **1998**, *179*, 64.

(17) Boccuti, M. R.; Rao, K. M.; Zecchina, A.; Leofanti, G.; Petrini, G. *Stud. Surf. Sci. Catal.* **1989**, *48*, 133.

(18) Zecchina, A.; Spoto, G.; Bordiga, S.; Padovan, M.; Leofanti, G. *Stud. Surf. Sci. Catal.* **1991**, *65*, 671.

(19) Scarano, D.; Zecchina, A.; Bordiga, S.; Geobaldo, F.; Spoto, G.; Petrini, G.; Leofanti, G.; Padovan, M.; Tozzola, G. *J. Chem. Soc., Faraday Trans.* **1993**, *89*, 4123.

(20) Deo, G.; Turek, A. M.; Wachs, I. E.; Huybrechts, D. R. C.; Jacobs, P. A. *Zeolites* **1993**, *13*, 365.

(21) Zecchina, A.; Spoto, G.; Bordiga, S.; Ferrero, A.; Petrini, G.; Padovan, M.; Leofanti, G. *Stud. Surf. Sci. Catal.* **1991**, *69*, 251.

(22) Huybrechts, D. R.; Buskens, P. L.; Jacobs, P. A. *J. Mol. Catal.* **1992**, *71*, 129.

(23) van der Pol, A. J. H. P.; van Hooff, J. H. C. *Appl. Catal. A.* **1992**, *92*, 93.

(24) Li, C.; Xiong, G.; Xin, Q.; Liu, J.; Ying, P.; Feng, Z.; Li, J.; Yang, W.; Wang, Y.; Wang, G.; Liu, X.; Lin, M.; Wang, X.; Min, E. *Angew. Chem., Int. Ed.* **1999**, *38*, 2220.

(25) Ricchiardi, G.; Damin, A.; Bordiga, S.; Lamberti, C.; Spanò, G.; Rivetti, F.; Zecchina, A. *J. Am. Chem. Soc.* **2001**, *121*, 11409.

(26) Blasco, T.; Camblor, M.; Corma, A.; Pérez-Parriente, J. *J. Am. Chem. Soc.* **1993**, *115*, 11806.

(27) Bordiga, S.; Coluccia, S.; Lamberti, C.; Marchese, L.; Zecchina, A.; Boscherini, F.; Buffa, F.; Genoni, F.; Leofanti, G.; Petrini, G.; Vlaic, G. *J. Phys. Chem.* **1994**, *98*, 4125.

(28) Bordiga, S.; Boscherini, F.; Coluccia, S.; Genoni, F.; Lamberti, C.; Leofanti, G.; Marchese, L.; Petrini, G.; Vlaic, G.; Zecchina, A. *Catal. Lett.* **1994**, *26*, 195.

(29) Pei, S.; Zajac, G. W.; Kaduk, J. A.; Faber, J.; Boyanov, B. I.; Duck, D.; Fazzini, D.; Morrison, T. I.; Yang, D. S. *Catal. Lett.* **1993**, *21*, 333.

(30) Le Noc, L.; Trong On, D.; Solomykina, S.; Echchahed, B.; Bel, F.; Cartier dit Moulin, C.; Bonneviot, L. *Stud. Surf. Sci. Catal.* **1996**, *101*, 611.

(31) Zecchina, A.; Bordiga, S.; Lamberti, C.; Ricchiardi, G.; Scarano, D.; Petrini, G.; Leofanti, G.; Mantegazza, M. *Catal. Today* **1996**, *32*, 97.

(32) Lamberti, C.; Bordiga, S.; Arduino, D.; Zecchina, A.; Geobaldo, F.; Spanò, G.; Genoni, F.; Petrini, G.; Carati, A.; Villain, F.; Vlaic, G. *J. Phys. Chem. B* **1998**, *102*, 6382.

(33) Trong On, D.; Le Noc, L.; Bonneviot, L. *Chem. Commun.* **1996**, 299.

(34) Lamberti, C.; Turnes Palomino, G.; Bordiga, S.; Arduino, D.; Zecchina, A.; Vlaic, G. *Jpn. J. Appl. Phys.* **1999**, *38-1*, 55.

(35) Gleeson, D.; Sankar, G.; Catlow, C. R. A.; Thomas, J. M. Spanò, G.; Bordiga, S.; Zecchina, A.; Lamberti, C. *Phys. Chem. Chem. Phys.* **2000**, *2*, 4812.

(36) Bolis, V.; Bordiga, S.; Lamberti, C.; Zecchina, A.; Petrini, G.; Rivetti, F.; Spanò, G. *Langmuir* **1999**, *155*, 753.

(37) Bolis, V.; Bordiga, S.; Lamberti, C.; Zecchina, A.; Petrini, G.; Rivetti, F.; Spanò, G. *Micropor. Mesopor. Mater.* **1999**, *30*, 67.

(38) Bordiga, S.; Geobaldo, F.; Lamberti, C.; Zecchina, A.; Boscherini, F.; Genoni, F.; Leofanti, G.; Petrini, G.; Padovan, M.; Geremia, S.; Vlaic, G. *Nucl. Instrum. Methods B* **1995**, *97*, 23.

(39) Millini, R.; Perego, G. *Gazz. Chim. Ital.* **1996**, *126*, 133.

(40) Vayssilov, G. N. *Catal. Rev. Sci. Eng.* **1997**, *39*, 209.

(41) Jentys, A.; Catlow, C. R. A. *Catal. Lett.* **1993**, *22*, 251.

(42) Millini, R.; Perego, G.; Seiti, K. *Stud. Surf. Sci.* **1994**, *84*, 2123.

(43) de Man, A. J. M.; Sauer, J. *J. Phys. Chem.* **1996**, *100*, 5025.

(44) Oumi, Y.; Matsuba, K.; Kubo, M.; Inui, T.; Miyamoto, A. *Micropor. Mater.* **1995**, *4*, 53.

(45) Smirnov, K. S.; van de Graaf, B. *Micropor. Mater.* **1996**, *7*, 133.

(46) Njo, S. L.; van Koningsveld, H.; van de Graaf, B. *J. Phys. Chem. B* **1997**, *101*, 10065.

(47) Sinclair, P. E.; Sankar, G.; Catlow, C. R. A.; Thomas, J. M.; Maschmeyer, T. *J. Phys. Chem. B* **1997**, *101*, 4237.

(48) Zicovich-Wilson, C. M.; Dovesi, R.; Corma, A. *J. Phys. Chem. B* **1999**, *103*, 988.

(49) Sinclair, P. E.; Catlow, C. R. A. *J. Phys. Chem. B* **1999**, *103*, 1084.

(50) Ricchiardi, G.; de Man, A.; Sauer, J. *Phys. Chem. Chem. Phys.* **2000**, *2*, 2195.

(51) Sinclair, P. E.; Sankar, G.; Catlow, C. R. A.; Thomas, J. M.; Maschmeyer, T. *J. Phys. Chem. B* **1997**, *101*, 4232.

(52) Munakata, H.; Oumi, Y.; Miyamoto, A. *J. Phys. Chem. B.* **2001**, *105*, 3493.

(53) Vayssilov, G. N.; van Santen R. A. *J. Catal.* **1998**, *175*, 170.

(54) (a) Zecchina, A.; Bordiga, S.; Spoto, G.; Marchese, L.; Petrini, G.; Leofanti, G.; Padovan, M. *J. Phys. Chem.* **1992**, *96*, 4985. (b) Zecchina, A.; Bordiga, S.; Spoto, G.; Marchese, L.; Petrini, G.; Leofanti, G.; Padovan, M. *J. Phys. Chem.* **1992**, *96*, 4991. (c) Zecchina, A.; Bordiga, S.; Spoto, G.; Marchese, L.; Petrini, G.; Leofanti, G.; Padovan, M.; Otero Areàn, C. *J. Chem. Soc., Faraday Trans.* **1992**, *88*, 2959. (d) Marra, G. L.; Tozzola, G.; Leofanti, G.; Padovan, M.; Petrini, G.; Genoni, F.; Venturelli, B.; Zecchina, A.; Bordiga, S.; Ricchiardi, G. *Stud. Surf. Sci. Catal.* **1994**, *84*, 559.

(55) Artioli, G.; Lamberti, C.; Marra, G. L. *Acta Crystallogr. B* **2000**, *56*, 2.

(56) (a) Bordiga, S.; Ugliengo, P.; Damin, A.; Lamberti, C.; Spoto, G.; Zecchina, A.; Spanò, G.; Buzzoni, R.; Dalloro, L.; Rivetti, F. *Top. Catal.* **2001**, *15*, 43. (b) Bordiga, S.; Roggero, I.; Ugliengo, P.; Zecchina, A.; Bolis, V.; Artioli, G.; Buzzoni, R.; Marra, G. L.; Rivetti, F.; Spanò, G.; Lamberti, C. *J. Chem. Soc., Dalton Trans.* **2000**, 3921.

(57) In the study of a Ti(IV)···NH_3···NH_3 interaction, the second ammonia molecule will interact also with the fraction of the cluster treated at low level in the embedded ONIOM scheme, so avoiding any significant comparison with the Ti(IV)···NH_3 case. The same holds for water molecules.

(58) Astorino, A.; Peri, J. B.; Willey, R. J.; Busca, G. *J. Catal.* **1995**, *157*, 482.

(59) Li, C.; Xiong, G.; Liu, J.; Ying, P.; Xin, Q.; Feng, Z. *J. Phys. Chem. B* **2001**, *105*, 2993.

(60) Bolis, V.; Cavenago, A.; Fubini, B. *Langmuir* **1997**, *13*, 895.

(61) Michalowicz, A. *J. Phys. IV Fr.* **1997**, *7*, C2−235.

(62) Lytle, F. W.; Sayers, D. E.; Stern, E. A *Physica B* **1989**, *158*, 701.

(63) (a) Zecchiana, A.; Bordiga, S.; Turnes Palomino, G.; Scarano, D.; Lamberti, C.; Salvalaggio, M. *J. Phys. Chem. B* **1999**, *103*, 3833. (b) Lamberti, C.; Turnes Palomino, G.; Bordiga, S.; Berlier G.; D'Acapito F.; Zecchina A. *Angew. Chem., Int. Ed. Engl.* **2000**, *39*, 2138.

(64) Ankudinov, A. L.; Ravel, B.; Rehr, J. J.; Conradson, S. D. *Phys. Rev. B* **1998**, *58*, 7565.

(65) Karlsen, E.; Schöffel, K. *Catal. Today* **1996**, *32*, 107.

(66) Neurock, M.; Manzer, L. *Chem. Commun.* **1996**, 1133.

(67) (a) Damin, A.; Bordiga, S.; Zecchina, A.; Lamberti, C. *J. Chem. Phys.* **2002**, *117*, 226. (b) Damin, A.; Bonino, F.; Ricchiardi, G.; Bordiga, S.; Zecchina, A.; Lamberti, C. *J. Phys. Chem. B* **2002**, *106*, 7524.

(68) (a) Maseras, F.; Morokuma, K. *J. Comput. Chem.* **1995**, *10*, 1170. (b) Humbel, S.; Sieber, S.; Morokuma, K. *J. Chem. Phys.* **1996**, *105*, 1959. (c) Dapprich, S.; Komaromi, I.; Byun, K. S.; Morokuma, K.; Frisch, M. J. *J. Mol. Struct. THEOCHEM* **1999**, *461*, 1.

(69) Hay, P. J.; Wadt, W. R. *J. Chem. Phys.* **1985**, *82*, 299.

(70) Schaefer, A.; Huber, C.; Ahlrichs, R. *J. Chem. Phys.* **1994**, *100*, 5829.

(71) Lendvay, G.; Mayer, I. *Chem. Phys. Lett.* **1998**, *297*, 365.

(72) Pazé, C.; Bordiga, S.; Lamberti, C.; Salvalaggio, M.; Zecchina A.; Bellussi, G. *J. Phys. Chem. B* **1997**, *101*, 4740.

(73) Zecchina, A.; Marchese, L.; Bordiga, S.; Pazè, C.; Gianotti, E. *J. Phys. Chem. B* **1997**, *101*, 10128.

(74) Zecchina, A.; Spoto, G.; Bordiga, S. Geobaldo, F. Petrini, G.; Leofanti, G.; Padovan, M.; Mantegazza, M.; Roffia, P. In *New Frontiers in Catalysis*; Guczi, L., Solymosi, F., Tétényi, P., Eds.; Elsevier: Amsterdam, 1993; p 719.

(75) Geobaldo, F.; Bordiga, S.; Zecchina, A.; Giamello, E.; Leofanti, G.; Petrini, G. *Catal. Lett.* **1992**, *16*, 109.

(76) Soult, A. S.; Poore, D. D.; Mayo, E. I.; Stiegman, A. E. *J. Phys. Chem. B* **2001**, *105*, 2687.

(77) In this regard, it is worth noting that the UV−vis spectrum with two distinct maxima around maximum 47 000 and 37 000 cm^{-1} reported in Figure 5 of ref 27 was obtained by dosing NH_4OH on TS-1 and not ammonia, as wrongly reported in the corresponding caption. We apologize for this error.

(78) Blasco, T.; Camblor, M. A.; Corma, A.; Esteve, P.; Guil, J. M.; Martinez, A.; Perdigon-Melon, J. A.; Valencia, S. J. *J. Phys. Chem. B* **1998**, *102*, 75.

(79) Carati, A.; Berti, D.; Mantegazza, M. A.; Stocchi, B.; Perego, G.; Bellussi, G.; Rivetti, F. Presented at EuropaCat V conference, Limerick (Ireland), September 2−7, 2001 (oral contribution 6-O-23).

(80) Bolis, V.; Busco, C.; Bordiga, S.; Ugliengo, P.; Lamberti, C.; Zecchina, A. *Appl. Surf. Sci.*, in press.

(81) The definition of α and β angles is straightforward in the presence of an adsorbed molecule (see section 2.3). However, the rupture of the T_d symmetry caused by embedding the $Ti(OSiH_3)_4$ unit in the zeolitic frameworks requires its definition for the bare CHA_T8 and MFI_T14 models also. In this case there is no preferential direction, so the splitting of the four O into three O_{eq} and one O_{ap} is arbitrary. To allow a direct comparison between the data reported in Tables 1 and 2, the O_{eq} and one O_{ap} in the bare cluster are defined as in the engaged clusters.

(82) Dovesi, R.; Saunders: V. R.; Roetti, C.; Causà, M.; Harrison, N. M.; Orlando, R.; Aprà, E. *CRYSTAL 95 User documentation*; University of Torino: Torino, 1995.

(83) At the end of section 4.2, the first multiple scattering simulation of the EXAFS signal of MFI_T16/H_2O and MFI_T16/NH_3 will be reported.

(84) Values obtained from more than 20 compounds extracted from the Cambridge Structure Data Bank.

(85) Eichler, U.; Brändle, M.; Sauer, J. *J. Phys. Chem. B* **1997**, *101*, 10035.